

Optimal bacteriophage mutation rates for phage therapy

David T. Kysela*, Paul E. Turner

Department of Ecology and Evolutionary Biology, Yale University, P.O. Box 208106, New Haven, CT 06520-8106, USA

Received 9 July 2006; received in revised form 10 August 2007; accepted 10 August 2007

Available online 25 August 2007

Abstract

The mutability of bacteriophages offers a particular advantage in the treatment of bacterial infections not afforded by other antimicrobial therapies. When phage-resistant bacteria emerge, mutation may generate phage capable of exploiting and thus limiting population expansion among these emergent types. However, while mutation potentially generates beneficial variants, it also contributes to a genetic load of deleterious mutations. Here, we model the influence of varying phage mutation rate on the efficacy of phage therapy. All else being equal, phage types with historical mutation rates of approximately 0.1 deleterious mutations per genome per generation offer a reasonable balance between beneficial mutational diversity and deleterious mutational load. We determine that increasing phage inoculum density can undesirably increase the peak density of a mutant bacterial class by limiting the in situ production of mutant phage variants. For phage populations with minimal genetic load, engineering mutation rate increases beyond the mutation–selection balance optimum may provide even greater protection against emergent bacterial types, but only with very weak selective coefficients for de novo deleterious mutations (below ~ 0.01). Increases to the mutation rate beyond the optimal value at mutation–selection balance may therefore prove generally undesirable.

© 2007 Elsevier Ltd. All rights reserved.

Keywords: Phage therapy; Mutation rate; Mutational load; Bacteriophage; Host range

1. Introduction

Phage therapy—the therapeutic application of bacteriophage to control bacterial infections—has recently sparked interest as a potential alternative or complement to more traditional antibiotic therapy. Phage therapy dates back to 1919, when d’Herelle (1926) first treated an outbreak of avian typhosis among farmed chickens. However, the approach was largely abandoned by Western science following the advent of clinical antibiotic treatment (Ho, 2001; Summers, 2001). The subsequent emergence of multi-drug resistant bacterial infections has provoked a resurgence in phage therapy (Thacker, 2003), with recent literature reviewing historical research (Alisky et al., 1998; Carlton, 1999; Chanishvili et al., 2001; Duckworth and Gulig, 2002; Ho, 2001; Sulakvelidze and Morris, 2001; Summers, 2001) and providing new theoretical and experimental results (Bull et al., 2002; Danelishvili et al.,

2006; Kasman et al., 2002; Levin and Bull, 1996; Matsuda et al., 2005; Merril et al., 1996; Payne and Jansen, 2001; Payne et al., 2000; Smith et al., 1987; Wagenaar et al., 2005; Watanabe et al., 2007; Weld et al., 2004; Xie et al., 2005).

Though phage and antibiotic therapy share the common objective of rapidly eradicating infective bacteria, several features distinguish these approaches. Phages are replicating biological entities capable of exponential population growth, whereas antibiotics cannot replicate in vivo. Phages also tend to infect a relatively limited range of bacterial hosts, unlike the broader killing spectrum obtained with most antibiotics. These and other attributes yield potential advantages and disadvantages to treatments employing phage or antibiotics. For example, the narrow killing spectrum afforded by phage permits selective elimination of infective bacteria without disrupting the remainder of the natural gut flora. However, the restrictive host range of many phages requires identification of the infectious bacterium and an appropriate phage—a potentially time-consuming process. Phage and antibiotics may thus function best as complementary, or even combined

*Corresponding author. Tel.: +1 203 432 7805; fax: +1 203 432 5176.
E-mail address: david.kysela@yale.edu (D.T. Kysela).

treatment options, rather than absolute alternatives (Schoolnik et al., 2004).

Phage mutation provides another potential advantage not afforded by antibiotics. Actively replicating phage give rise to mutants that may successfully eliminate emergent bacterial types resistant to the phage population initially administered. Experimental manipulation of phage polymerases and accessory proteins even permits direct modification of phage mutation rates (Bebenek et al., 2002; Dressman et al., 1997; Kroutil et al., 1998; Kunkel et al., 1994). Antibiotics, on the other hand, are static molecules incapable of selectively responding to resistant bacteria in vivo. Levin and Bull (2004) highlighted the potential advantage of phage mutations to phage therapy, offering a simulation of how mutant phage might limit resistant bacteria. However, no study to date has thoroughly explored the impact of various phage mutation rates on the efficacy of therapeutic phage treatment.

The variation afforded to populations through mutations acts as a double-edged sword. On the one hand, mutations provide the raw material (variation) for adaptation to changing conditions. For phage populations, host range mutations can provide the opportunity to exploit otherwise resistant bacterial hosts. On the other hand, most mutations of meaningful effect are deleterious and therefore depress the mean fitness of a population by increasing mutational load (Haldane, 1937). Any particular mutation rate thus strikes a balance between the advantages of evolutionary flexibility and the costs of deleterious mutational load (Haldane, 1937; Wright, 1932).

Here, we examine quantitatively the influence of phage mutation rate in the context of phage therapy. We present a mathematical model that accounts for the emergence of bacteria resistant to the inoculated phage population, as well as mutant phage capable of exploiting this emergent bacterial type. Our results point to particular phage mutation rate values that maximize the therapeutic effect of potential host range mutations within the phage population, while minimizing the deleterious consequences of mutational load.

2. Theory and methods

2.1. General model and assumptions

Our model of bacteria and bacteriophage dynamics extends previous phage therapy models to include bacterial mutations in phage susceptibility and phage mutations in host range. We modify population dynamic equations from Levin and Bull (1996) by ignoring the effects of immune response and antibiotics. We assume free mixing of bacteria and phage with density-independent bacterial growth and no passive mortality (although we shall later relax this assumption). We fix phage burst size (β) at 100, adsorption rate (δ) at $2 \times 10^{-9} \text{ ml h}^{-1}$, and bacterial growth rate (ψ) at 1 h^{-1} . These parameter values roughly agree

with those employed in other phage therapy models (Levin and Bull, 1996; Payne and Jansen, 2001; Weld et al., 2004). Mean phage fitness, \bar{w}_i , exercises its effect directly on phage reproduction, and a phage population free of deleterious mutations has a fitness of unity on its appropriate bacterial host. In order to focus directly on mutational effects, we ignore latent period (the time lag between phage adsorption and release of phage progeny) and keep model parameters constant across mutational classes and conditions (but see Weld et al., 2004).

An initial bacterial population (B_0) and phage population (P_0) give rise to the emergent classes B_1 and P_1 via mutation. We represent the densities of bacterial class B_i and phage class P_i at time t as the italicized terms B_i and P_i , respectively, with initial densities $B_i(0)$ and $P_i(0)$. Bacteria mutate between classes at rate μ_B , and we take no specific account of their mutational load. We set a phage genomic deleterious mutation rate of μ_P . Host range mutations result in a shift between phage classes, with a ratio γ of host range mutations per deleterious mutation. Initial densities of the emergent populations reflect these mutation rates: $B_1(0) = \mu_B B_0(0)$ and $P_1(0) = \mu_P P_0(0)$. Phage of class P_0 only infect bacteria of class B_0 , failing to attach to B_1 bacteria. P_1 phage experience an expanded host range, infecting B_0 and B_1 bacteria with equal efficiency. Initial mutation of B_0 bacteria to B_1 thus affords resistance to the initial P_0 phage type, and phage mutation from P_0 to P_1 permits exploitation of the emergent B_1 bacterial population.

Given the above assumptions, the following time-differential equations describe rates of change in the bacterial and phage populations:

$$\frac{dB_0}{dt} = \psi B_0(1 - \mu_B) + \psi B_1 \mu_B - \delta B_0(P_0 + P_1), \quad (1)$$

$$\frac{dB_1}{dt} = \psi B_1(1 - \mu_B) + \psi B_0 \mu_B - \delta B_1 P_1, \quad (2)$$

$$\frac{dP_0}{dt} = \delta \bar{w}_0 B_0 P_0 \beta + \delta \bar{w}_1 (B_0 + B_1) P_1 \beta \mu_P \gamma, \quad (3)$$

$$\frac{dP_1}{dt} = \delta \bar{w}_1 (B_0 + B_1) P_1 \beta + \delta \bar{w}_0 B_0 P_0 \beta \mu_P \gamma. \quad (4)$$

Following Levin and Bull (1996), our analysis shall focus on the ability of phage to limit peak bacterial density as a metric of the severity of bacterial infection.

2.2. Mutation–selection balance model

For populations evolving over long periods at a particular mutation rate, an equilibrium load of deleterious alleles arises at the point where introduction of alleles by mutation matches their elimination via selection. Assuming an equilibrium mutational load of alleles with multiplicative fitness effects across many loci in the phage genome results in a phage fitness of proportion $e^{-\mu_P}$ of that of a non-mutating phage (Haldane, 1937; Johnson, 1999;

Kimura and Maruyama, 1966). At mutation–selection equilibrium, a constant mean fitness thus applies to each phage population:

$$\bar{w}_0 = \bar{w}_1 = e^{-\mu_p}. \quad (5)$$

Substituting Eq. (5) into Eqs. (3) and (4) permits interpretation of the population dynamic model at mutation–selection balance.

We now wish to determine the peak density of individual bacterial populations. Each bacterial class experiences a period of exponential expansion and collapse, supporting the expansion of its corresponding phage population during a defined period (see Results and discussion). During each such period, the alternate bacterial population density remains low, due either to insufficient time for population expansion from a lower starting density (B_1 during B_0 expansion) or to eradication by previous phage predation (B_0 during B_1 expansion). Accordingly, when integrating strictly over these periods, we can effectively ignore the influence of the alternate bacterial population on the populations of interest. We therefore combine the rate equations for B_i and P_i , neglecting those terms involving the alternate bacterial population, to obtain the separable equation:

$$(\delta e^{-\mu_p} \beta) dB_i \approx \left(\frac{\psi}{P_i} - \delta \right) dP_i. \quad (6)$$

Integrating up to the time (\hat{t}_i) of peak bacterial density (\hat{B}_i), one obtains

$$\hat{B}_i \approx \frac{(\psi/\delta) \ln(P_i(\hat{t}_i)/P_i(\text{init})) - P_i(\hat{t}_i) + P_i(\text{init})}{\beta e^{-\mu_p}} + B_i(\text{init}) \quad (7)$$

with $B_i(\hat{t}_j)$ and $P_i(\hat{t}_j)$ indicating densities of bacterial and phage populations i at peak density of bacterial population j . The term \hat{B}_i provides a simplified notation for $B_i(\hat{t}_i)$, the peak density of bacterial population i . $t = \text{init}$ denotes the start of the interval of interest. In calculating \hat{B}_0 , init indicates the time of inoculation. For \hat{B}_1 , init denotes the time point immediately after elimination of the initial bacterial class via phage predation. Setting the derivative of bacterial population density in Eqs. (1) and (2) equal to zero gives the phage density at peak density of the corresponding bacterial class, denoted by $P_i(\hat{t}_i)$:

$$P_0(\hat{t}_0) \approx \frac{\psi}{\delta} \left((1 - \mu_B) + \frac{B_1(\hat{t}_0)\mu_B}{\hat{B}_0} \right) - P_1(\hat{t}_0) \quad (8)$$

$$P_1(\hat{t}_1) \approx \frac{\psi}{\delta} \left((1 - \mu_B) + \frac{B_0(\hat{t}_1)\mu_B}{\hat{B}_1} \right) \quad (9)$$

Again noting the low density of the alternate bacterial population, and that $P_0 \gg P_1$ at peak density of the B_0 population and $\mu_B \ll 1$, we obtain the simple approximation

$$P_i(\hat{t}_i) \approx \frac{\psi}{\delta} \quad (10)$$

For $P_i(\hat{t}_i)$ in Eq. (7)

$$\hat{B}_i \approx \frac{\psi}{\delta e^{-\mu_p} \beta} \left(\ln \left[\frac{\psi}{\delta P_i(\text{init})} \right] - 1 + \frac{\delta P_i(\text{init})}{\psi} \right) + B_i(\text{init}). \quad (11)$$

In typical phage therapy studies, $P_i(\hat{t}_i)$ greatly exceeds the phage inoculum density. Under such conditions, where $\psi/\delta \gg P_i(\text{init})$ and peak bacterial density vastly exceeds initial density, we can eliminate small terms and reduce Eq. (11):

$$\hat{B}_i \approx \frac{\psi}{\delta e^{-\mu_p} \beta} \left(\ln \left[\frac{\psi}{\delta P_i(\text{init})} \right] - 1 \right). \quad (12)$$

This solution thus demonstrates the peak bacterial concentration’s sensitivity to phage inoculum and insensitivity to initial bacterial density observed in numerical simulations by Levin and Bull (1996). Conversely, when $\psi/\delta \leq P_i(0)$, the corresponding bacterial population declines immediately, resulting in “passive therapy”. In such a scenario, setting the derivative of Eq. (1) or (2) equal to zero no longer provides an accurate solution for \hat{B}_i (the initial derivative is negative), but, quite simply, $\hat{B}_i = B_i(0)$.

While initial P_0 phage inoculum allows us to solve for \hat{B}_0 , determining the initial density of P_1 in order to solve for \hat{B}_1 is less straightforward. Since an obvious time lag exists between the collapse of B_0 and the expansion of B_1 (see Results and discussion), we take the results following the B_0 population collapse as inputs to our model of B_1 population dynamics. We integrate Eq. (6) to obtain the density of the initial phage class over the period of B_0 population expansion and collapse:

$$P_0 \approx \frac{\psi}{\delta} \ln \left(\frac{P_0}{P_0(0)} \right) + P_0(0) - e^{-\mu_p} \beta (B_0 - B_0(0)), \quad (13)$$

which we then solve by numerical methods. We are specifically interested in the value of P_0 at the time of B_0 population collapse, which we denote by \check{t} . Since our continuous model prevents absolute elimination, we define \check{t} to occur when B_0 drops below unity. Noting that B_0 effectively declines to zero at \check{t} , we find that

$$P_0(\check{t}) \approx \frac{\psi}{\delta} \ln \left(\frac{P_0(\check{t})}{P_0(0)} \right) + P_0(0) - e^{-\mu_p} \beta (B_0(0)). \quad (14)$$

When $\psi/\delta \gg P_0(0)$ (i.e., therapy is not passive), $P_0(\check{t}) \gg P_0(0)$ due to in situ phage reproduction. Also considering the large value of the reciprocal δ^{-1} (typical adsorption rates are on the order of 10^{-8} – 10^{-9} ml h $^{-1}$; Levin et al., 1977; Weld et al., 2004), the first term on the right-hand side of Eq. (14) yields much larger values than the remaining terms, resulting in the following approximation for the non-passive therapy scenario:

$$P_0(\check{t}) \approx \frac{\psi}{\delta} \ln \left(\frac{P_0(\check{t})}{P_0(0)} \right). \quad (15)$$

Because B_0 bacteria are effectively eliminated well before expansion of the B_1 population (see Results and discussion), expansion of the P_0 phage population effectively

terminates with the B_0 collapse. Additions to the P_1 phage class over this interval occur through mutation from P_0 and infection of B_0 bacteria by P_1 phage. As above, in determining \hat{B}_i , we ignore the influence of the minor B_1 population over this interval, combining the remaining terms in Eqs. (3) and (4) to obtain the separable equation:

$$\begin{aligned} &(\delta\bar{w}_1 B_0 P_1 \beta + \delta\bar{w}_0 B_0 P_0 \beta \mu_p \gamma) dP_0 \\ &\approx (\delta\bar{w}_0 B_0 P_0 \beta + \delta\bar{w}_1 B_0 P_1 \beta \mu_p \gamma) dP_1. \end{aligned} \quad (16)$$

Because $P_1 \ll P_0$ over this interval and we consider only low mutation rates between phage classes ($\gamma \leq 10^{-5}$), we can eliminate the small term containing the product $P_1 \gamma$ to obtain the following approximation:

$$(\delta\bar{w}_1 B_0 P_1 \beta + \delta\bar{w}_0 B_0 P_0 \beta \mu_p \gamma) dP_0 \approx (\delta\bar{w}_0 B_0 P_0 \beta) dP_1. \quad (17)$$

Since the phage populations share a common mutational load at mutation–selection balance, we can equate \bar{w}_0 and \bar{w}_1 . Eliminating common terms from Eq. (17), multiplying both the sides by the integrating factor P_0^{-1} , and integrating provide a useful approximation for P_1 over the interval of B_0 population expansion and collapse:

$$P_1 \approx P_0 \left(\mu_p \gamma \ln \left[\frac{P_0}{P_0(0)} \right] + \frac{P_1(0)}{P_0(0)} \right). \quad (18)$$

Substituting the numerical value of $P_0(\tilde{t})$ determined by Eq. (14) for P_0 solves for P_1 following the B_0 bacterial population crash and before the emergence of the B_1 population:

$$P_1(\tilde{t}) \approx P_0(\tilde{t}) \left(\mu_p \gamma \ln \left[\frac{P_0(\tilde{t})}{P_0(0)} \right] + \frac{P_1(0)}{P_0(0)} \right). \quad (19)$$

This solution accounts for P_1 phage from three sources: introduction at the time of inoculation ($P_1(0)$), infection of the B_0 population by P_1 phage, and mutations occurring during expansion of the initial phage class, P_0 . We thus treat $P_1(\tilde{t})$ as $P_1(\text{init})$ in solving \hat{B}_1 using Eq. (11).

We explored the impact of mutation rate under the mutation–selection balance model using numerical integration and approximate analytical solutions from the above equations. Numerical solutions resulted from integration in Mathematica (Wolfram Research, Inc., 2005) of the time-differential model of Eqs. (1)–(4), substituting Eq. (5) for phage fitness. Approximate analytical solutions for \hat{B}_i utilized Eq. (11), substituting Eq. (19) for initial phage density in the case of \hat{B}_1 . The FindMinimum function in Mathematica (Wolfram Research, Inc., 2005) identified minimum values for \hat{B}_1 across mutation rates and γ values.

2.3. Multiple emergent population classes

To determine the behavior of the model when extended to multiple mutational classes, we consider generalized population dynamic equations:

$$\frac{dB_i}{dt} = \psi B_i(1 - \mu_B) + \psi B_{i-1} \mu_B - \delta B_i \left(\sum_{j \geq i} P_j \right), \quad (20)$$

$$\frac{dP_i}{dt} = \delta \bar{w}_i \left(\sum_{j \leq i} B_j \right) P_i \beta + \delta \bar{w}_{i-1} \left(\sum_{k < i} B_k \right) P_{i-1} \beta \mu_p \gamma. \quad (21)$$

For simplicity, these equations consider only sequential mutation from each phage and bacterial population to a subsequent mutational class, without back mutation to the previous class. We observed the behavior of this extended model by numerical integration using Mathematica (Wolfram Research, Inc., 2005).

2.4. Phage mortality

We explore the influence of phage mortality, encompassing any sources of phage elimination, by incorporating a constant elimination rate parameter, λ . The phage population dynamic equations (3) and (4) are thus extended to include an extra term representing phage loss:

$$\frac{dP_0}{dt} = \delta \bar{w}_0 B_0 P_0 \beta + \delta \bar{w}_1 (B_0 + B_1) P_1 \beta \mu_p \gamma - \lambda P_0, \quad (22)$$

$$\frac{dP_1}{dt} = \delta \bar{w}_1 (B_0 + B_1) P_1 \beta + \delta \bar{w}_0 B_0 P_0 \beta \mu_p \gamma - \lambda P_1. \quad (23)$$

Eqs. (1) and (2), describing bacterial population dynamics, remain unchanged, representing a lack of passive bacterial mortality in this model. The inclusion of the phage mortality dynamic prohibits the analytical approach explored in the previous section. We therefore explored the system behavior by numerical integration using Mathematica (Wolfram Research, Inc., 2005) and by stochastic simulations (see below).

2.5. Simulations

To examine the behavior of our system in a stochastic setting, we simulated bacteria and phage populations interacting according to the dynamics defined by our model in Eqs. (1)–(4). Phage infection events occurred according to a random binomial sample with probability determined by population densities and the adsorption rate δ , as in Eqs. (1) and (2). Elimination of individual phage followed a random binomial sampling process with probability determined by the loss rate parameter, λ , as in Eqs. (22) and (23). All simulations used a total system volume of 11.

The simulation program binned phage into 1001 discrete relative fitness classes ranging from 0 to 1, or 2001 fitness classes from 0 to 2 when allowing beneficial mutations, with relative fitness of 1 for the mutation-free genotype. Mutations between classes (for bacteria and phage) and deleterious mutations (for phage) were generated by random sampling from a Poisson distribution at rates defined by the model parameters. For the mixed mutational effect model (see Results and discussion), mutations were first randomly assigned lethal, beneficial, or non-lethal deleterious effect based on the relative frequency of each class. Non-lethal deleterious mutations were further

assigned a magnitude by randomly sampling a four-category approximation of a negative binomial distribution.

For simulations with phage populations beginning at mutation–selection balance, we first generated stationary fitness distributions by simulating extended reproduction in an infinite resource environment. Starting from a population free of deleterious mutations, we permitted mutation accumulation until mean fitness change per generation declined below 0.02% of the expected mutational load (i.e., $0.0002 \cdot e^{-\mu_P}$). Initial phage populations were then seeded according to the stationary distribution corresponding to the same mutation rate and distribution of mutational effects.

All simulations were programmed in C++ and compiled using GNU g++ 4.0. Source code is available from the authors on request.

3. Results and discussion

3.1. Mutation–selection balance

Under the mutation–selection balance model, initial expansion and subsequent phage-mediated collapse occur in the first bacterial population (B_0), followed by a similar

pattern in the second bacterial population (B_1) (Fig. 1). This observation agrees with results from previous phage therapy models (Levin and Bull, 1996, 2004; Payne and Jansen, 2001; Weld et al., 2004). The magnitude of μ_B influences the timing of the B_1 population expansion, but not its peak density (Fig. 1(a) and (c)). On the other hand, increases in μ_P result in a decreased peak density of the emergent bacterial population (\hat{B}_1) for values of μ_P below approximately 0.1 deleterious mutations per genome per generation. Little change in the peak density of the initial bacterial population (\hat{B}_0) occurs over this same range (Figs. 1(a) and (b) and 2).

The model behavior at phage deleterious mutation rates below 0.1 mutations per genome per generation agrees intuitively with previous observations on phage therapy model dynamics. In the absence of mutation, greater bacterial inoculum density results in an earlier bacterial population peak, but has little influence on peak bacterial density. Conversely, higher phage inoculum density reduces peak bacterial density, but the timing of peak bacterial density remains unchanged (Levin and Bull, 1996). In our mutation–selection balance model, similar patterns are observed for the mutant bacterial (B_1) and phage (P_1) classes, except that higher bacterial and phage

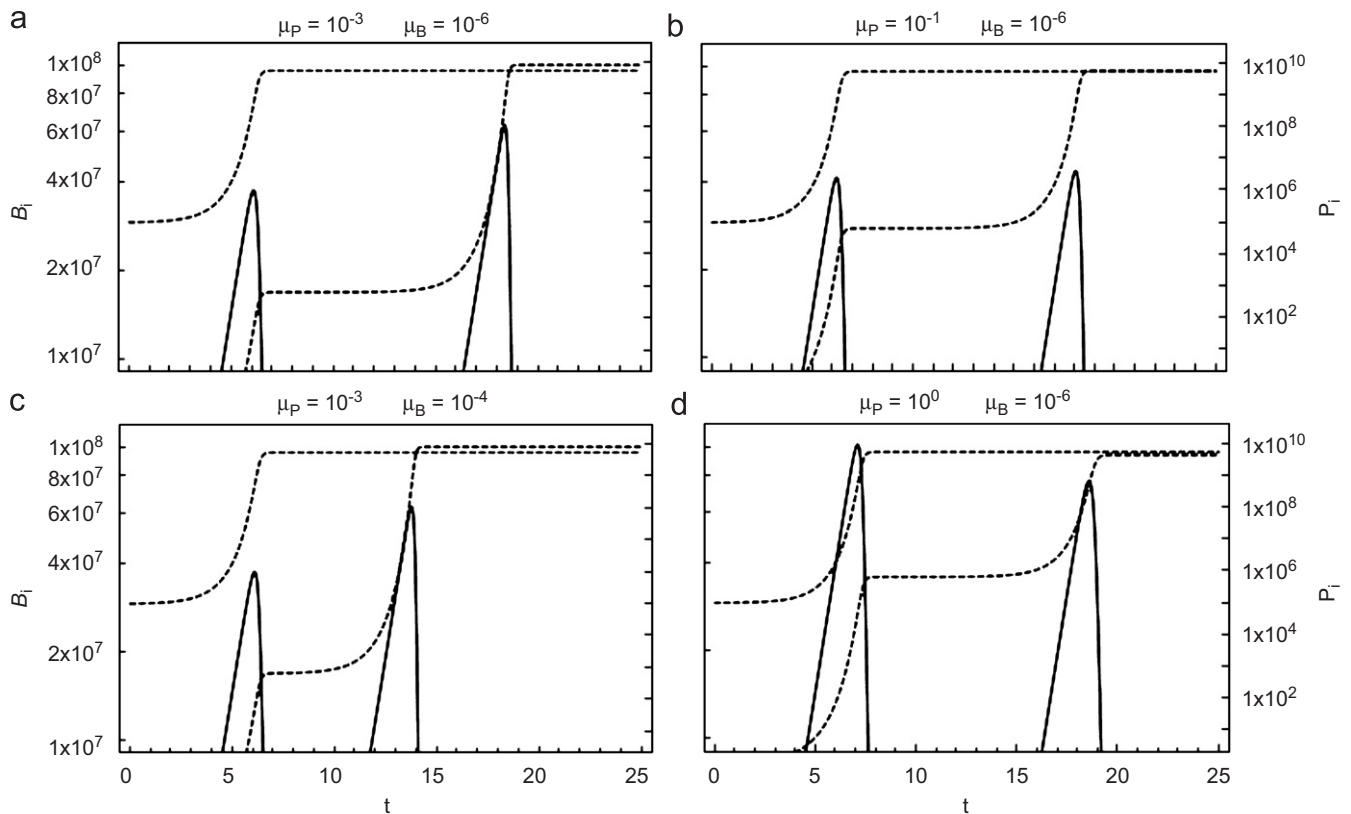


Fig. 1. Phage mutation rate impacts the magnitude of emergent bacterial peak population density (\hat{B}_1), but not its timing. Panels represent separate numerical solutions of bacterial and phage population densities at varying mutation rates. Solid curves represent bacterial population densities (left y-axis), with the B_0 class spiking first in each panel, followed by B_1 . Dashed curves represent the associated phage population densities (right y-axis), with P_0 expanding first, then P_1 . μ_P indicates phage deleterious mutation rate per genome per generation; μ_B indicates the per generation mutation rate between bacterial classes. In order to emphasize key differences, the y-axis does not span the full range of observed densities. For all panels, $\beta = 100$, $\delta = 2 \times 10^{-9} \text{ ml h}^{-1}$, $\psi = 1 \text{ h}^{-1}$, $\gamma = 10^{-5}$, $B_0(0) = 10^5 \text{ ml}^{-1}$, and $P_0(0) = 10^5 \text{ ml}^{-1}$.

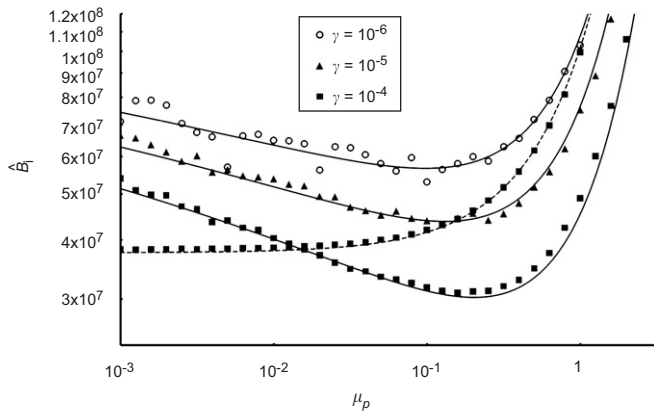


Fig. 2. Intermediate phage mutation rates minimize peak density of the mutant bacterial class. Dashed and solid curves indicate analytical solution peak densities of the initial (\hat{B}_0) and the mutant (\hat{B}_1) bacterial populations, respectively, for various phage mutation rates. Symbols represent stochastic simulation results with a mixed distribution of both lethal and exponentially distributed non-lethal deleterious mutations (see text for details). $\beta = 100$, $\delta = 2 \times 10^{-9} \text{ ml h}^{-1}$, $\psi = 1 \text{ h}^{-1}$, $\mu_B = 10^{-6}$, $B_0(0) = 10^5 \text{ ml}^{-1}$, and $P_0(0) = 10^5 \text{ ml}^{-1}$.

mutation rates effectively increase the “inoculum” densities of the respective populations. For example, a higher phage mutation rate results in more mutant (P_1) phage production from initial (P_0) phage population growth, thereby reducing the peak density (\hat{B}_1) of the emergent bacterial population (Fig. 2).

As phage deleterious mutation rate (μ_P) increases much beyond 0.1 mutations per genome per generation, peak population density in both B_0 and B_1 increases substantially (Figs. 1(d) and 2). At these high mutation rates, the increased mutant phage density still tends to reduce the emergent bacterial population, but this effect is overwhelmed by low phage fitness resulting from excessive mutational load. This negative fitness effect of mutation manifests itself at all mutation rates, as evidenced by the monotonic increase in the peak density of the initial bacterial population with increased mutation rate (Fig. 2).

We simulated the behavior of the mutation–selection balance model in a stochastic setting for comparison with our analytical results. Simulation outcomes demonstrate somewhat greater variance in \hat{B}_1 at the lowest mutation rates examined, particularly with low proportions of host range mutations, γ (Fig. 2). This pattern reflects random fluctuations in the relatively low number of P_1 phage produced during the expansion of the P_0 phage population at low values of the host range mutation rate $\gamma\mu_P$. Nonetheless, the results confirm our analytical solutions under the mutation–selection balance scenario, demonstrating a similar relationship between phage mutation rate and peak bacterial densities.

Thus, a tradeoff occurs at intermediate mutation rates: as phage mutation rate increases, peak density increases for the initial bacterial class and decreases for the emergent class. This tradeoff disappears at very high mutation rates as peak density increases for both bacterial classes with

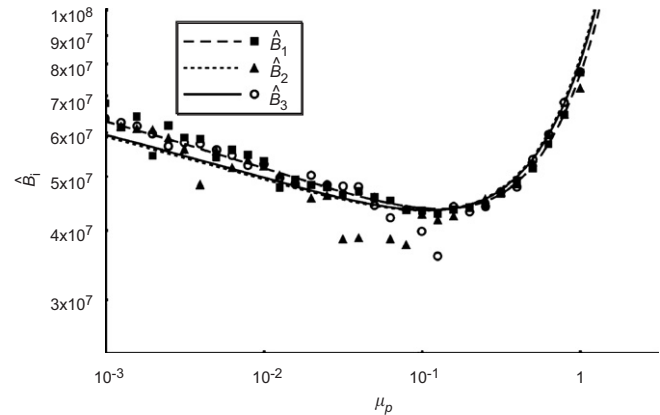


Fig. 3. The phage mutation rate resulting in minimum peak bacterial densities remains consistent during co-evolution. Curves indicate peak densities of mutant bacterial populations as determined by numerical integration. Symbols represent stochastic simulation results with a mixed distribution of both lethal and exponentially distributed non-lethal deleterious mutations (see text for details). $\beta = 100$, $\delta = 2 \times 10^{-9} \text{ ml h}^{-1}$, $\psi = 1 \text{ h}^{-1}$, $\mu_B = 10^{-6}$, $B_0(0) = 10^5 \text{ ml}^{-1}$, and $P_0(0) = 10^5 \text{ ml}^{-1}$.

further increases in phage mutation rate (Fig. 2). This threshold mutation rate, which minimizes emergent bacterial peak density (\hat{B}_1), increases slightly as the ratio of beneficial to deleterious mutations (γ) increases, from 0.096 to 0.198 mutations per phage genome per generation for γ of 10^{-6} and 10^{-4} , respectively. This shift in mutational threshold results because higher proportions of beneficial mutations mitigate the mutational load more effectively. Nonetheless, we emphasize that, even across a broad range of γ values, the minimal peak density of the emergent bacterial population occurs across a relatively limited range of phage mutation rates.

The results above consider only one initial and one mutant class for both phage and bacteria. Several empirical studies identify multiple rounds of bacterial mutation to resistance and subsequent phage host range expansion to include the mutant types (Buckling and Rainey, 2002; Lenski and Levin, 1985; Mizoguchi et al., 2003). We therefore extended the mutation–selection balance model to include multiple mutant phage and bacterial classes. In this scenario, subsequent bacterial mutants emerge sequentially from previous classes, resulting in a repeated pattern of bacterial population expansion and collapse, separated in time (data not shown). Minimum peak bacterial densities occur at the same mutation rate observed in the two-class model (Fig. 3). The similarity of this result to the two-class case demonstrates that the tradeoff between variability and mutational load remains quantitatively consistent even with extended co-evolution.

3.2. Influence of mutational effect at mutation–selection balance

Returning to the two-class model at mutation–selection balance, we examined mutations with different distributions

of fitness effects using stochastic simulations (data not shown). In particular, we compared populations encountering two types of uniform mutational effects: low cost (1% fitness reduction) and moderate cost (10% fitness reduction). We also considered a distribution with large, mixed effects similar to observations of Sanjuán et al. (2004). In this case, exponentially distributed non-lethal mutations with a 25% mean fitness reduction (mean selection coefficient $\bar{s} = -0.25$) accounted for 45% of deleterious mutations, with lethal mutations accounting for the remaining 55% ($s = -1$). In all the cases, we first generated stationary fitness distributions at mutation–selection balance via extended reproduction. These then served as the starting fitness distributions for inoculating phage populations in phage therapy simulations.

None of these mutational distributions influences the outcome observed in Fig. 2, which shows simulation results only from the mixed distribution (data not shown). This result confirms previous conclusions indicating that the magnitude of deleterious mutational load at mutation–selection balance depends strictly on the mutation rate and not on mutational effect (Haldane, 1937; Johnson, 1999; Kimura and Maruyama, 1966). We therefore restrict further simulation results to the mixed model of mutational effects, except in the case of populations beginning out of equilibrium (see below). However, results obtained at mutation–selection balance apply regardless of the shape and magnitude of the underlying deleterious mutation distribution.

3.3. Inoculation density

While in situ mutation provides new phage genotypes for controlling resistant bacterial types, we also expect mutational variants to occur among the inoculating phage population. We might therefore anticipate that increasing the inoculum density would help to limit the size of the emergent bacterial population (B_1) by introducing a larger pool of mutant phage, effectively increasing the inoculum density of the emergent phage class (P_1).

Contrary to this argument, for most realistic inoculum densities, the peak density of the emergent bacterial population actually increases with larger phage inoculum density (Fig. 4). Consideration of Eqs. (11) and (19) reveals the problem: higher inoculum densities result in lower emergent phage class densities (P_1) following the collapse of the initial bacterial population. Specifically, when the initial phage population limits its bacterial host population to a lower peak density, the phage population experiences less opportunity for reproduction. The final density of the initial phage population ($P_0(\bar{t})$) therefore decreases, as does the final input into the emergent phage class via mutation during reproductive events. Thus, the effective “inoculum” of the P_1 phage class decreases, permitting a higher peak density of the emergent bacterial population. A tradeoff thus occurs between the peak density of the initial bacterial class (\hat{B}_0) and that of the emergent class (\hat{B}_1): higher

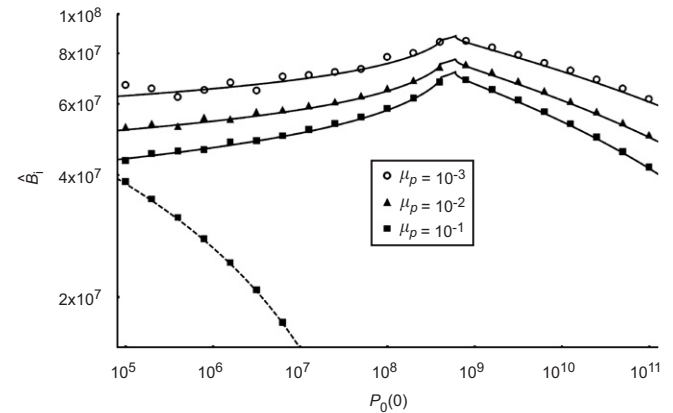


Fig. 4. Increasing phage inoculum can increase emergent bacterial population density. Dashed and solid curves indicate analytical solutions to peak densities of the initial (\hat{B}_0) and mutant (\hat{B}_1) bacterial populations, respectively, for various phage inoculum densities ($P_0(0)$). \hat{B}_0 curves are nearly identical for $\mu_p < 10^{-1}$ (data not shown); for clarity, the plot includes the \hat{B}_0 curve only for $\mu_p = 10^{-2}$. Symbols represent stochastic simulation results with a mixed distribution of lethal and exponentially distributed non-lethal deleterious mutational effects. $\beta = 100$, $\delta = 2 \times 10^{-9} \text{ ml h}^{-1}$, $\psi = 1 \text{ h}^{-1}$, $\mu_B = 10^{-6}$, $B_0(0) = 10^5 \text{ ml}^{-1}$, and $P_0(0) = 10^5 \text{ ml}^{-1}$.

inoculum densities tend to reduce \hat{B}_0 (as previously concluded by Levin and Bull, 1996) while also increasing \hat{B}_1 (Fig. 4).

For very high inoculation densities, a reversal in this pattern occurs as the peak density of the emergent bacterial class declines with higher initial phage density (Fig. 4). At this point, sufficient densities of the emergent phage class in the inoculum compensate for the lack of in situ reproduction. These densities generally exceed those employed experimentally (Geier et al., 1973; Merrill et al., 1996; Smith and Huggins, 1982). If such large inoculations proved feasible, passive treatment of the initial bacterial class and effective control of the emergent class could both occur without a performance tradeoff.

3.4. Phage mortality

Our initial model assumes no passive phage loss; once produced, phage remain in the system indefinitely. However, phage titers often decline rapidly in the inoculated host, particularly due to phagocytosis by the host immune system (Geier et al., 1973). Extended evolution in the therapeutic environment can greatly extend phage persistence, thereby maintaining high phage titers during the course of the treatment (Merrill et al., 1996). Nonetheless, we examined the interaction between the phage mortality and the mutation rate for phage experiencing high rates of elimination.

Although phage mortality tends to reduce the effectiveness of phage in limiting peak densities of both the initial and the emergent bacterial classes, the influence of mutation remains essentially the same as in the absence of phage elimination (Fig. 5). The phage mutation rate

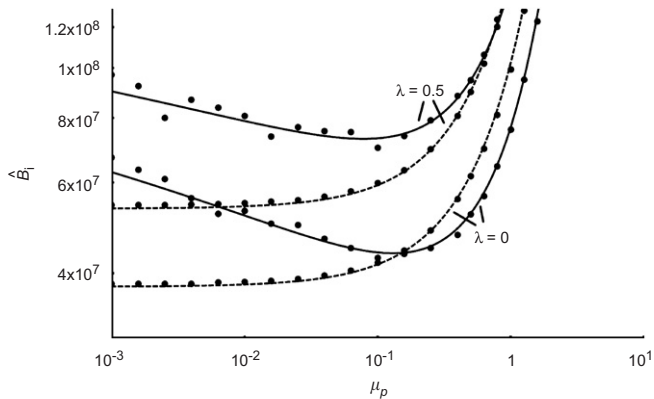


Fig. 5. Phage mortality has little influence on the optimal phage mutation rate at mutation–selection balance. Dashed and solid curves indicate peak densities of the initial (\hat{B}_0) and the mutant (\hat{B}_1) bacterial populations, respectively, for specific phage elimination rates (λ) as determined by numerical integration. Filled circles represent stochastic simulation results with both lethal and exponentially distributed non-lethal deleterious mutational effects. $\beta = 100$, $\delta = 2 \times 10^{-9} \text{ ml h}^{-1}$, $\psi = 1 \text{ h}^{-1}$, $\mu_B = 10^{-6}$, $\gamma = 10^{-5}$, $B_0(0) = 10^5 \text{ ml}^{-1}$, and $P_0(0) = 10^5 \text{ ml}^{-1}$.

resulting in the lowest density of the emergent bacterial population does decrease slightly to just below 10^{-1} for the high loss rate ($50\% \text{ h}^{-1}$) depicted in Fig. 5, while the difference becomes less pronounced as the loss rate decreases (data not shown). In this sense, phage loss represents an additional “load” on the population beyond the fitness cost of deleterious mutation. Thus, a slight reduction occurs in the critical mutation rate at which the negative consequences of load outweigh the advantages afforded by increased mutational variability.

The inclusion of phage mortality in the model also introduces periodic cycling in the mutant bacterial and phage population densities (Volterra, 1926). One potential drawback to increasing phage mutation rate involves a corresponding increase in the frequency of population expansion and collapse cycles. Higher phage mutation rate results in decreased peak bacterial density, thereby sustaining less phage reproduction during each bacterial population expansion. As the bacterial population declines, fewer phage remain to scavenge residual bacteria, resulting in a higher effective bacterial “inoculum” for the following population expansion: earlier bacterial re-emergence and thus increased cycling frequency results (data not shown). Such effects prove unimportant in situations where phage completely eradicate mutant bacteria following the first population expansion, but the outcome depends on the model parameter values. In particular, high phage mortality rates will favor bacterial persistence between cycles, as rapid elimination of phage hinders eradication of residual bacteria (data not shown).

3.5. Novel mutation rate

For phage therapy applications, elevating the phage mutation rate might prove desirable in order to promote

the capacity of mutant phage to limit emergent bacteria that are resistant to the initial phage type. Indeed, it appears possible to achieve elevated phage mutation rates by introducing a low-fidelity DNA polymerase (Bebenek et al., 2002; Dressman et al., 1997; Kroutil et al., 1998; Kunkel et al., 1994), even from distantly related phage types (Dressman et al., 1997; Wang et al., 1995).

In such cases with a novel, elevated mutation rate, phage populations may begin out of mutation–selection balance, then approach the equilibrium mutational load as population expansion proceeds. This approach to equilibrium proceeds asymptotically over a number of generations, with the rate of approach dependent on the magnitude and the distribution of deleterious mutations (Johnson, 1999). Historical mutation rates below 0.005 mutations per genome per generation typical of double-stranded DNA phages (Drake, 1991) should result in a miniscule mutational load according to Eq. (5). For simplicity, we therefore examined scenarios with no mutational load in the initial phage population.

Phage populations beginning without mutational load continue to limit peak bacterial density effectively at higher mutation rates than observed above for populations at mutation–selection balance (Fig. 6). Since these elevated mutation rates result in higher “inoculum” densities of the emergent phage class, peak densities of the mutant bacterial class can be reduced even further than in the mutation–selection balance scenario above (Figs. 2 and 6; note that $\gamma = 10^{-5}$ in Fig. 6). Higher fitness costs of individual deleterious mutations hasten the approach of phage fitness to the equilibrium value $e^{-\mu_p}$ (Johnson, 1999), as evidenced by poorer phage performance (i.e., higher peak bacterial densities) at similar mutation rates as mutational fitness effect increases (Fig. 6).

Given this observed impact of mutational effect on the efficacy of highly elevated mutation rates, it becomes particularly important to determine the empirical character of de novo mutations. Many estimates of the average effect of deleterious mutation yield selective coefficients roughly in the range of 10^{-2} – 10^{-1} across a broad taxonomic range of organisms (Burch and Chao, 2004; Elena and Moya, 1999; Lynch et al., 1999; Schultz et al., 1999; Vassilieva et al., 2000). At the low end of this range of mutational effects ($s = 10^{-2}$), phage performance improves against the emergent bacterial population for increases in phage mutation rates up to approximately one deleterious mutation per phage genome per generation.

Despite the potential advantages of increased mutation rates when deleterious mutations cause relatively minor fitness effects, the studies cited above rely on offspring survival for estimating fitness, failing to account for lethal mutations that could greatly increase the average mutational effect. A study of mutational effects in vesicular stomatitis virus (VSV) by Sanjuán et al. (2004) permitted observation of lethal mutations; as discussed above, their analysis arrived at a de novo mutational distribution with

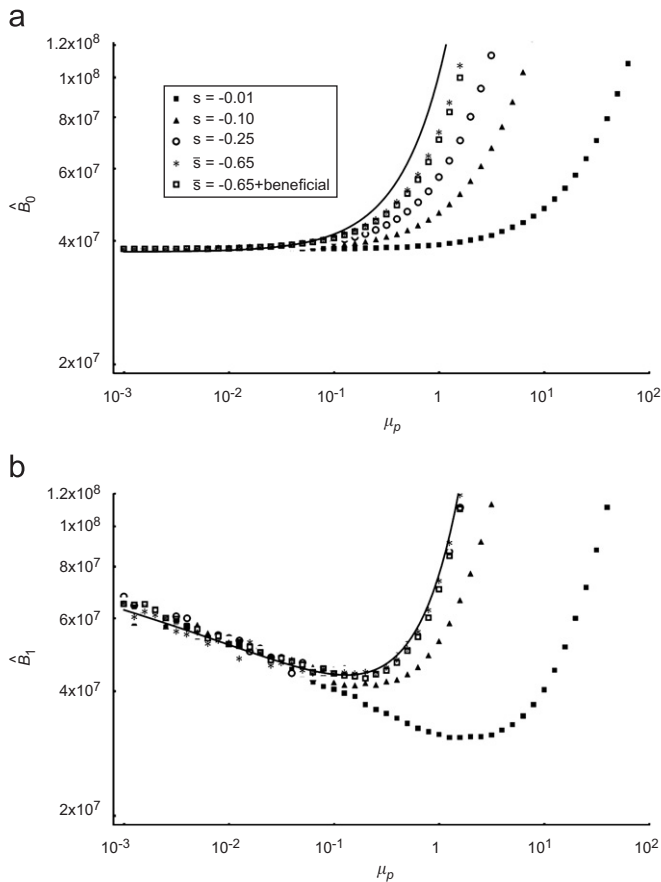


Fig. 6. Manipulation of historically low phage mutation rates further limits the peak density of the mutant bacteria only with low mutational effects. Symbols indicate peak densities of the bacterial populations observed in the simulations for various magnitudes of deleterious mutational effect (s). Solid curves indicate analytical results at mutation–selection balance. $\bar{s} = -0.65$ denotes a mixed model of lethal exponentially distributed deleterious mutations, whereas $\bar{s} = -0.65 + \text{beneficial}$ denotes an extension of the mixed model that includes beneficial mutations (see text for details). Phage populations start without mutational load. (a) Peak density of the initial bacterial class (\hat{B}_0). (b) Peak density of the mutant bacterial class (\hat{B}_1). In both the plots, $\beta = 100$, $\delta = 2 \times 10^{-9} \text{ ml h}^{-1}$, $\psi = 1 \text{ h}^{-1}$, $\mu_B = 10^{-6}$, $\gamma = 10^{-5}$, $B_0(0) = 10^5 \text{ ml}^{-1}$, and $P_0(0) = 10^5 \text{ ml}^{-1}$.

a high proportion of lethal mutations, with a mean relative fitness cost of $\sim 65\%$ among the combined pool of lethal and non-lethal deleterious mutations. When applied to our simulations, this distribution results in an extremely rapid approach to mutation–selection balance, with the outcome differing little from phage populations initiated at equilibrium (Fig. 6).

The inclusion of beneficial mutations occurring at a frequency of 5% relative to the deleterious mutation rate, as observed in the VSV study (Sanjuán et al., 2004), fails to slow the approach to equilibrium noticeably (Fig. 6). Note that, for consistency, we still define μ_p solely according to deleterious mutation rate rather than overall mutation rate, which would include neutral and beneficial mutations. In terms of results from Sanjuán et al. (2004), overall mutation rate is 1.45 times our deleterious mutation rate,

which includes only their “lethal” and “deleterious” mutation categories.

Our reliance on the mutation effect distribution observed for VSV highlights a clear need for detailed mutational study in other organisms. In particular, the high mutation rate observed for the RNA-based VSV, estimated at 1.2 deleterious mutations per genome per generation (Elena and Moya, 1999), may result in a mutation profile fundamentally distinct from DNA-based viruses, with typical mutation rate estimates below 0.005 mutations per genome and generation (Drake, 1991; Drake et al., 1998). Interestingly, evolution at high mutation rates should tend to increase mutational robustness (Montville et al., 2005; Wilke et al., 2001), thereby reducing the effect of new mutations. If other organisms prove equally or even more susceptible to deleterious mutational effects than VSV, the rapid approach to the equilibrium genetic load observed above could apply generally, limiting the therapeutic value of further increases in the mutation rate beyond the optimum at mutation–selection balance.

3.6. Implications for phage therapy design

Our results offer suggestions for the initial selection and engineering of phages applied therapeutically. First, for phages at mutation–selection balance, we observe optimal performance at historical mutation rates around 10^{-1} deleterious mutations per genome per generation. Phages with extremely high mutation rates may perform poorly in a phage therapy context due to excessive deleterious mutational load. Certain RNA-based phages with mutation rates in excess of 0.1 mutations per genome per generation (de la Peña et al., 2000; Domingo et al., 1978; Drake, 1993; Drake and Holland, 1999) may therefore represent poor phage therapy candidates, although mutation rates in some RNA phages may lie just below this threshold (Burch and Chao, 2004). Conversely, phages with much lower mutation rates gain little reduction in the mutational load, but fail to limit the mutant bacterial types as effectively as their moderately mutable counterparts. We caution that these conclusions are derived specifically from mutation rate considerations; other factors, such as phage virulence and burst size, will influence therapeutic efficacy (Levin and Bull, 1996) and may vary substantially between phage types.

Second, increases in phage mutation rate can help to minimize further the peak density of the emergent bacterial types. Mutational load effects take time to accumulate in populations with low historical load, extending the useful range of phage mutation rates beyond values observed in the mutation–selection balance scenario. However, the magnitude of this advantage depends on the fitness effects of deleterious mutations, requiring selection coefficients that may prove unrealistically low. As such, engineered increases in the mutation rate up to 0.1 deleterious mutations per genome and generation appear advantageous, while further increases may prove undesirable.

Our model presents convenient simplifications of mutant phenotypes that fail to reflect certain biological details. We assume that phage-resistant bacterial mutants maintain population dynamics similar to the initial bacterial class. In fact, the competitive ability of phage-resistant types can decline in chemostat experiments (Bohannon and Lenski, 2000; Lenski and Levin, 1985). Similarly, phage performance may vary across the range of bacterial hosts (Duffy et al., 2006). Extension of the model to reflect variable interaction dynamics (e.g., variable adsorption rates) between classes (Weitz et al., 2005) might provide therapeutically relevant insights.

In certain cases, bacteria appear to develop absolute resistance that phage mutation cannot overcome (Bohannon and Lenski, 1997, 1999; Lenski and Levin, 1985). The benefits of mutation observed in our analyses would then disappear. However, details of phage resistance and host range mutations remain unknown for many bacterial pathogens and their corresponding phages. Given this uncertainty and the relatively minor mutational load for mutation rates below 10^{-1} deleterious mutations per genome per generation, the potential advantages merit the application of a moderately mutable phage type.

In the cases where phages target virulence factors, phage resistance can attenuate bacterial virulence (Smith and Huggins, 1982). Indeed, the selection of the phage known a priori to target virulence factors provides a rational phage therapy design choice to sidestep the problem of bacterial mutation (Levin and Bull, 2004). As with host range, virulence and competitive ability of phage-resistant bacteria remain poorly understood in most cases. We therefore reiterate the advantage of intermediate phage mutation rates in the absence of such details.

4. Conclusions

Our results provide the first quantitative analysis of the impact of the phage mutation rate on phage therapy. We have determined that mutation rates of approximately 10^{-1} deleterious mutations per phage genome per generation provide a desirable balance between beneficial variation and deleterious mutational load at mutation–selection balance. Further mutation rate increases in populations with little historical load offer an advantage only in the case of extremely small mutational effect. We have also found that increasing phage inoculum densities can actually reduce therapeutic efficacy against the emergent bacterial types by reducing the density of the mutant phage, despite advantages in eliminating the initial bacterial type. Thorough understanding of phage interactions with bacterial fitness, particularly with respect to virulence factors, can limit the threats posed to phage therapy by bacterial mutation. However, our model offers quantitative guidelines for rational phage therapy design in the absence of complete information.

Acknowledgments

We thank Ed Kaplan for assistance in initial model development and Steve Abedon and members of the Turner Lab for useful discussions. An anonymous reviewer provided valuable feedback on an earlier draft of the paper. This material is based upon work supported under a National Science Foundation Graduate Research Fellowship to D.T.K. The National Institutes of Health Predoctoral Training Program in Genetics (NIH T32 GM07499) and the Cyberinfrastructure for Phylogenetic Research Project provided additional support.

References

- Alisky, J., Iczkowski, K., Rapoport, A., Troitsky, N., 1998. Bacteriophages show promise as antimicrobial agents. *J. Infect.* 36, 5–15.
- Bebenek, A., Carver, G.T., Dressman, H.K., Kadyrov, F.A., Haseman, J.K., Petrov, V., Konigsberg, W.H., Karam, J.D., Drake, J.W., 2002. Dissecting the fidelity of bacteriophage RB69 DNA polymerase: site-specific modulation of fidelity by polymerase accessory proteins. *Genetics* 162, 1003–1018.
- Bohannon, B.J.M., Lenski, R.E., 1997. The effect of resource enrichment on a chemostat community of bacteria and phage. *Ecology* 78, 2303–2315.
- Bohannon, B.J.M., Lenski, R.E., 1999. Effect of prey heterogeneity on the response of a model food chain to resource enrichment. *Am. Nat.* 153, 73–82.
- Bohannon, B.J.M., Lenski, R.E., 2000. Linking genetic change to community evolution: insights from studies of bacteria and bacteriophage. *Ecol. Lett.* 3, 362–377.
- Buckling, A., Rainey, P.B., 2002. Antagonistic coevolution between a bacterium and a bacteriophage. *Proc. Biol. Sci.* 269, 931–936.
- Bull, J.J., Levin, B.R., DeRouin, T., Walker, N., Bloch, C.A., 2002. Dynamics of success and failure in phage and antibiotic therapy in experimental infections. *BMC Microbiol.* 2, 35.
- Burch, C.L., Chao, L., 2004. Epistasis and its relationship to canalization in the RNA virus ϕ 6. *Genetics* 167, 559–567.
- Carlton, R.M., 1999. Phage therapy: past history and future prospects. *Arch. Immunol. Ther. Exp.* 47, 267–274.
- Chanishvili, N., Chanishvili, T., Tediashvili, M., Barrow, P.A., 2001. Phages and their application against drug-resistant bacteria. *J. Chem. Technol. Biotechnol.* 76, 689–699.
- d’Herelle, F., 1926. *The Bacteriophage and its Behavior*. Williams and Wilkins, Baltimore.
- Danelishvili, L., Young, L.S., Bermudez, L.E., 2006. In vivo efficacy of phage therapy for *Mycobacterium avium* infection as delivered by a nonvirulent mycobacterium. *Microb. Drug Resist.* 12, 1–6.
- de la Peña, M., Elena, S.F., Moya, A., 2000. Effect of deleterious mutation-accumulation on the fitness of RNA bacteriophage MS2. *Evolution* 54, 686–691.
- Domingo, E., Sabo, D., Taniguchi, T., Weissmann, C., 1978. Nucleotide sequence heterogeneity of an RNA phage population. *Cell* 13, 735–744.
- Drake, J.W., 1991. A constant rate of spontaneous mutation in DNA-based microbes. *Proc. Natl Acad. Sci. USA* 88, 7160–7164.
- Drake, J.W., 1993. Rates of spontaneous mutation among RNA viruses. *Proc. Natl Acad. Sci. USA* 90, 4171–4175.
- Drake, J.W., Holland, J.J., 1999. Mutation rates among RNA viruses. *Proc. Natl Acad. Sci. USA* 96, 13910–13913.
- Drake, J.W., Charlesworth, B., Charlesworth, D., Crow, J.F., 1998. Rates of spontaneous mutation. *Genetics* 148, 1667–1686.
- Dressman, H.K., Wang, C.C., Karam, J.D., Drake, J.W., 1997. Retention of replication fidelity by a DNA polymerase functioning in a distantly related environment. *Proc. Natl Acad. Sci. USA* 94, 8042–8046.

- Duckworth, D.H., Gulig, P.A., 2002. Bacteriophages: potential treatment for bacterial infections. *Biodrugs* 16, 57–62.
- Duffy, S., Turner, P.E., Burch, C.L., 2006. Pleiotropic costs of niche expansion in the RNA bacteriophage ϕ 6. *Genetics* 172, 751–757.
- Elena, S.F., Moya, A., 1999. Rate of deleterious mutation and the distribution of its effects on fitness in vesicular stomatitis virus. *J. Evol. Biol.* 12, 1078–1088.
- Geier, M.R., Trigg, M.E., Merrill, C.R., 1973. Fate of bacteriophage lambda in non-immune germ-free mice. *Nature* 246, 221–223.
- Haldane, J.B.S., 1937. The effect of variation on fitness. *Am. Nat.* 71, 337–349.
- Ho, K., 2001. Bacteriophage therapy for bacterial infections. Rekindling a memory from the pre-antibiotics era. *Perspect. Biol. Med.* 44, 1–16.
- Johnson, T., 1999. The approach to mutation–selection balance in an infinite asexual population, and the evolution of mutation rates. *Proc. Biol. Sci.* 266, 2389–2397.
- Kasman, L.M., Kasman, A., Westwater, C., Dolan, J., Schmidt, M.G., Norris, J.S., 2002. Overcoming the phage replication threshold: a mathematical model with implications for phage therapy. *J. Virol.* 76, 5557–5564.
- Kimura, M., Maruyama, T., 1966. The mutational load with epistatic gene interactions in fitness. *Genetics* 54, 1337–1351.
- Kroutil, L.C., Frey, M.W., Kaboord, B.F., Kunkel, T.A., Benkovic, S.J., 1998. Effect of accessory proteins on T4 DNA polymerase replication fidelity. *J. Mol. Biol.* 278, 135–146.
- Kunkel, T.A., Patel, S.S., Johnson, K.A., 1994. Error-prone replication of repeated DNA sequences by T7 DNA polymerase in the absence of its processivity subunit. *Proc. Natl Acad. Sci. USA* 91, 6830–6834.
- Lenski, R.E., Levin, B.R., 1985. Constraints on the coevolution of bacteria and virulent phage: a model, some experiments, and predictions for natural communities. *Am. Nat.* 125, 585–602.
- Levin, B.R., Bull, J.J., 1996. Phage therapy revisited: the population biology of a bacterial infection and its treatments with bacteriophage and antibiotics. *Am. Nat.* 147, 881–898.
- Levin, B.R., Bull, J.J., 2004. Population and evolutionary dynamics of phage therapy. *Nat. Rev. Microbiol.* 2, 166–173.
- Levin, B.R., Stewart, F.M., Chao, L., 1977. Resource-limited growth, competition, and predation—a model and experimental studies with bacteria and bacteriophage. *Am. Nat.* 111, 3–24.
- Lynch, M., Blanchard, J., Houle, D., Kibota, T., Schultz, S., Vassilieva, L., Willis, J., 1999. Perspective: spontaneous deleterious mutation. *Evolution* 53, 645–663.
- Matsuda, T., Freeman, T.A., Hilbert, D.W., Duff, M., Fuortes, M., Stapleton, P.P., Daly, J.M., 2005. Lysis-deficient bacteriophage therapy decreases endotoxin and inflammatory mediator release and improves survival in a murine peritonitis model. *Surgery* 137, 639–646.
- Merrill, C.R., Biswas, B., Carlton, R., Jensen, N.C., Creed, G.J., Zullo, S., Adhya, S., 1996. Long-circulating bacteriophage as antibacterial agents. *Proc. Natl Acad. Sci. USA* 93, 3188–3192.
- Mizoguchi, K., Morita, M., Fischer, C.R., Yoichi, M., Tanji, Y., Unno, H., 2003. Coevolution of bacteriophage PP01 and *Escherichia coli* O157:H7 in continuous culture. *Appl. Environ. Microbiol.* 69, 170–176.
- Montville, R., Froissart, R., Remold, S.K., Tenailon, O., Turner, P.E., 2005. Evolution of mutational robustness in an RNA virus. *PLoS Biol.* 3, e381.
- Payne, R.J., Jansen, V.A., 2001. Understanding bacteriophage therapy as a density-dependent kinetic process. *J. Theor. Biol.* 208, 37–48.
- Payne, R.J., Phil, D., Jansen, V.A., 2000. Phage therapy: the peculiar kinetics of self-replicating pharmaceuticals. *Clin. Pharm. Ther.* 68, 225–230.
- Sanjuán, R., Moya, A., Elena, S.F., 2004. The distribution of fitness effects caused by single-nucleotide substitutions in an RNA virus. *Proc. Natl Acad. Sci. USA* 101, 8396–8401.
- Schoolnik, G.K., Summers, W.C., Watson, J.D., 2004. Phage offer a real alternative. *Nat. Biotechnol.* 22, 505–506.
- Schultz, S.T., Lynch, M., Willis, J.H., 1999. Spontaneous deleterious mutation in *Arabidopsis thaliana*. *Proc. Natl Acad. Sci. USA* 96, 11393–11398.
- Smith, H.W., Huggins, M.B., 1982. Successful treatment of experimental *Escherichia coli* infections in mice using phage: its general superiority over antibiotics. *J. Gen. Microbiol.* 128, 307–318.
- Smith, H.W., Huggins, M.B., Shaw, K.M., 1987. The control of experimental *Escherichia coli* diarrhoea in calves by means of bacteriophages. *J. Gen. Microbiol.* 133, 1111–1126.
- Sulakvelidze, A., Morris Jr., J.G., 2001. Bacteriophages as therapeutic agents. *Ann. Med.* 33, 507–509.
- Summers, W.C., 2001. Bacteriophage therapy. *Ann. Rev. Microbiol.* 55, 437–451.
- Thacker, P.D., 2003. Set a microbe to kill a microbe: drug resistance renews interest in phage therapy. *J. Am. Med. Assoc.* 290, 3183–3185.
- Vassilieva, L.L., Hook, A.M., Lynch, M., 2000. The fitness effects of spontaneous mutations in *Caenorhabditis elegans*. *Evolution* 54, 1234–1246.
- Volterra, V., 1926. Variations and fluctuations of the numbers of individuals in animal species living together. *J. Cons. Int. Explor. Mer* 3, 3–51.
- Wagenaar, J.A., Van Bergen, M.A., Mueller, M.A., Wassenaar, T.M., Carlton, R.M., 2005. Phage therapy reduces *Campylobacter jejuni* colonization in broilers. *Vet. Microbiol.* 109, 275–283.
- Wang, C.C., Yeh, L.S., Karam, J.D., 1995. Modular organization of T4 DNA polymerase. Evidence from phylogenetics. *J. Biol. Chem.* 270, 26558–26564.
- Watanabe, R., Matsumoto, T., Sano, G., Ishii, Y., Tateda, K., Sumiyama, Y., Uchiyama, J., Sakurai, S., Matsuzaki, S., Imai, S., Yamaguchi, K., 2007. Efficacy of bacteriophage therapy against gut-derived sepsis caused by *Pseudomonas aeruginosa* in mice. *Antimicrob. Agents Chemother.* 51, 446–452.
- Weitz, J.S., Hartman, H., Levin, S.A., 2005. Coevolutionary arms races between bacteria and bacteriophage. *Proc. Natl Acad. Sci. USA* 102, 9535–9540.
- Weld, R.J., Butts, C., Heinemann, J.A., 2004. Models of phage growth and their applicability to phage therapy. *J. Theor. Biol.* 227, 1–11.
- Wilke, C.O., Wang, J.L., Ofria, C., Lenski, R.E., Adami, C., 2001. Evolution of digital organisms at high mutation rates leads to survival of the flattest. *Nature* 412, 331–333.
- Wolfram Research, Inc., 2005. *Mathematica 5.2*. Champaign, IL.
- Wright, S., 1932. The roles of mutation, inbreeding, crossbreeding, and selection in evolution. In: *Proceedings of the VI International Congress of Genetics*, pp. 356–366.
- Xie, H., Zhuang, X., Kong, J., Ma, G., Zhang, H., 2005. Bacteriophage Esc-A is an efficient therapy for *Escherichia coli* 3-1 caused diarrhea in chickens. *J. Gen. Appl. Microbiol.* 51, 159–163.